ACS APPLIED MATERIALS & INTERFACES

Research Article

www.acsami.org

Polystyrene Nanofiber Materials for Visible-Light-Driven Dual Antibacterial Action via Simultaneous Photogeneration of NO and $O_2(^1\Delta_g)$

Jiří Dolanský,[†,‡] Petr Henke,[†] Pavel Kubát,[§] Aurore Fraix,[∥] Salvatore Sortino,*[,∥] and Jiří Mosinger*[,†,‡]

[†]Faculty of Science, Charles University in Prague, 2030 Hlavova, 128 43 Prague 2, Czech Republic

[‡]Institute of Inorganic Chemistry, v.v.i., Czech Academy of Sciences, 250 68 Řež, Czech Republic

[§]J. Heyrovský Institute of Physical Chemistry, v.v.i., Czech Academy of Sciences, Dolejškova 3, 182 23 Prague 8, Czech Republic

[∥]Laboratory of Photochemistry, Department of Drug Sciences, University of Catania, Viale Andrea Doria 6, I-95125 Catania, Italy

Supporting Information

ABSTRACT: This contribution reports on the preparation, characterization, and biological evaluation of electrospun polystyrene nanofiber materials engineered with a covalently grafted NO photodonor and ionically entangled tetracationic porphyrin and phthalocyanine photosensitizers. These photofunctional materials exhibit an effective and simultaneous photogeneration of two antibacterial species such as nitric oxide (NO) and singlet oxygen, $O_2(^1\Delta_g)$ under illumination with visible light, as demonstrated by their direct detection using amperometric and time-resolved spectroscopic techniques. Dual-mode photoantibacterial action is demonstrated by antibacterial tests carried out on *Escherichia coli*.

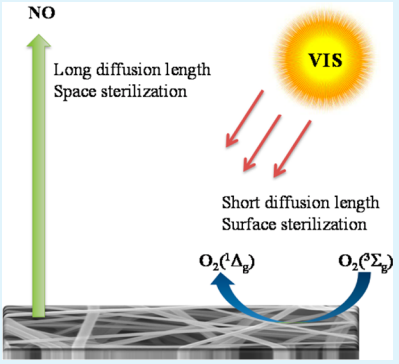

KEYWORDS: *nanofiber, singlet oxygen, nitric oxide, photogeneration, antibacterial*

INTRODUCTION

The development of electrospun polymeric nanofiber materials as wound dressings, temporary skin applications, filtration materials, water disinfection materials, and scaffolds for tissue engineering is becoming a subject of both academic and commercial interest because of the unique characteristics of nanofiber materials. These include high specific area, excellent porosity and absorption capacity, and tunable mechanical properties.[1−5]

In contrast to nanoparticles, nanofiber materials consist of nanofibers with diameters in the range of nanometers to a few micrometers but with lengths that can range up to a few meters. Individual nanofibers are connected to each other, and they form compact materials similar to a textile. Therefore, nanofiber materials are generally not considered to be as toxic as nanoparticles.

Recently, we prepared photoactive polymeric nanofiber materials with encapsulated porphyrinoid photosensitizers that generate the short-lived and highly cytotoxic $O_2(^1\Delta_g)$ in high quantum yield upon irradiation with visible light.[6−10] The typical diameter of the nanofibers (ca. 100−400 nm) and the oxygen permeability of the selected polymers (polyurethane, polystyrene (PS), and polycaprolactone)[8] allow efficient diffusion of $O_2(^1\Delta_g)$ outside of the nanofibers, followed by photooxidation of the chemical/biological targets. Therefore, these nanofiber materials exhibited a strong antibacterial and virucidal effect on their surface. The nanoporous structure of nanofiber membranes[1,11] also prevents the bacteria from passing through, thus detaining them on the material's surface.[12,13] The common feature of the polymeric nanofiber materials with a photosensitizer is a short diffusion length for the $O_2(^1\Delta_g)$ (typically tens to hundreds of nm),[14] which limits the efficient antibacterial action to close proximity to the nanofiber surface, especially in aqueous media where $O_2(^1\Delta_g)$ has a short lifetime (3.5 μs[15]). The lifetime of $O_2(^1\Delta_g)$ in other solvents is reported in literature.[16] This limitation can be overcome by attaching a photosensitizer to the nanofiber surface[12,17] or by increasing the wettability of the surface.[18] In contrast to nanofiber materials with encapsulated photosensitizer, the $O_2(^1\Delta_g)$ molecules photogenerated from photosensitizers bound to the nanofiber surface diffuse over a shorter distance to the target molecules; however, the properties of the photosensitizers, e.g., ability to generate $O_2(^1\Delta_g)$, are strongly influenced by the environment.

Alternatively, nanofibers can be modified by grafting a longer-lived antibacterial agent with a longer diffusion length. Nitric oxide (NO) fits both of these requirements. Indeed, this inorganic free radical has a lifetime of approximately 4 s in air

Received: July 10, 2015
Accepted: October 2, 2015
Published: October 2, 2015

DOI: 10.1021/acsami.5b06233
ACS Appl. Mater. Interfaces 2015, 7, 22980−22989

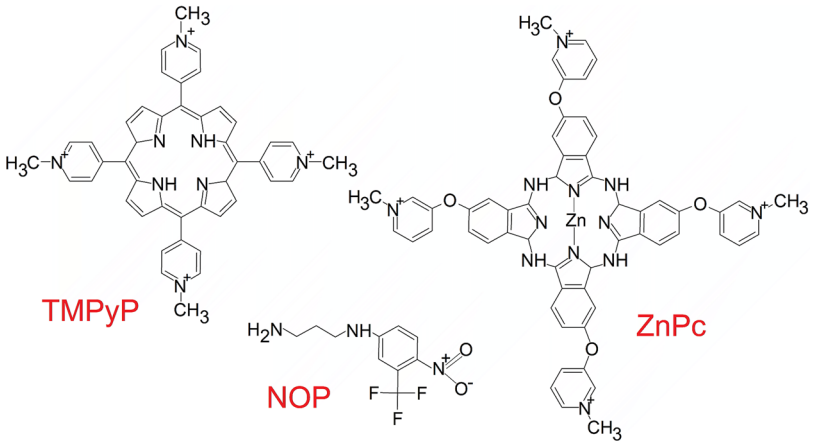

Figure 1. Structures of the photoactive compounds used in this work: NO photodonor (NOP), tetracationic TMPyP and tetracationic ZnPc photosensitizers.

and a diffusion radius of approximately 100 μm. Similar to $O_2(^1\Delta_g)$, NO is characterized by small size, absence of charge, multitarget therapeutic capability with a broad spectrum of antibacterial activity,[19] and absence of multidrug resistance problems that are encountered with several conventional target-specific drugs. The gaseous delivery of NO to selected targets has motivated the development of a range of molecular NO donors[20,21] and photodonors,[22−24] and their incorporation within a variety of materials for biomedical applications has been achieved in recent years.[25,26] Additionally, nanofiber materials with covalently attached S-nitrosothiols (NO donors) have been prepared via thiolation or S-nitrosation of the poly(lactic-*co*-glycolic-*co*-hydroxymethyl propionic acid) and subsequently electrospun. The resulting material exhibited a strong antibacterial effect.[27]

Therefore, the combination of $O_2(^1\Delta_g)$ with NO represents an ideal strategy in view of bimodal antibacterial treatments. The objective of this study was the fabrication of nanofiber materials that combined a suitable NO photodonor with $O_2(^1\Delta_g)$ photosensitizers to exploit the possible synergistic/additive antibacterial effects due to the simultaneous photogeneration of these two antibacterial agents. The high surface area and the nanoporous structure of nanofiber materials are advantages that provide a high concentration of photoactive compounds and prevent bacteria and other pathogens from passing through the nanofiber materials because they are detained on the surface and killed by the photogenerated NO and $O_2(^1\Delta_g)$. To our knowledge, multifunctional nanofiber materials that simultaneously photogenerate NO and $O_2(^1\Delta_g)$ on the surface have not yet been investigated.

Our approach involves the covalent binding of the NO photodonor and electrostatic binding of the $O_2(^1\Delta_g)$ photosensitizer on the surface of electrospun PS nanofiber materials. We used *N*-(3-aminopropyl)-3-(trifluoromethyl)-4-nitrobenzenamine (NOP) as a suitable NO photodonor[28] and 5,10,15,20-tetrakis(*N*-methylpyridinium-4-yl)porphyrin tetra-*p*-toluensulfonate (TMPyP) and zinc(II) 2,9,16,23-tetrakis(*N*-methyl-pyridiumoxy)phthalocyanine tetraiodide (ZnPc) as the $O_2(^1\Delta_g)$ photosensitizers (Figure 1).[29,30] The choice of these chromophoric units was motivated by our recent work that demonstrated that NO photodonors based on this nitroaniline derivative and the porphyrinoid photosensitizers "ignore" each other once they are colocalized within the same compartment of different 2D and 3D nanoconstructs.[26,31−35] This allows both chromophores to behave as independent units and, as a consequence, to operate in parallel under light inputs. Additionally, the choice of two photosensitizers with different absorption spectra should allow the control of the photogeneration of $O_2(^1\Delta_g)$ by the selection of the appropriate excitation light energy.

EXPERIMENTAL SECTION

Chemicals. 5,10,15,20-Tetrakis(*N*-methylpyridinium-4-yl)-porphyrin tetra-*p*-toluensulfonate (TMPyP), uric acid, cyclohexanone, tetraethylammonium bromide (TEAB), 1,3-propyldiamine, 4-chloro-2-(trifluoromethyl)-1-nitrobenzene, chlorosulfonic acid, deuterium oxide, 2,3-diaminonaphthalene (DAN), myoglobin (Mb, from equine heart), ampicillin sodium salt, potassium iodide, and sodium hydrosulfite were purchased from Sigma-Aldrich. LB agar (Lennox) and LB media (Lennox) were purchased from Carl Roth GmbH & Co., Germany. The photosensitizer zinc(II) 2,9,16,23-tetrakis(*N*-methyl-pyridiumoxy)phthalocyanine tetraiodide (ZnPc, sum of isomers) was purchased from COC s.r.o., Czech Republic. PS (Synthos PS GP 137) was purchased from Synthos Kralupy a.s., Czech Republic. Dichloromethane, hydrochloric acid, ethanol, and methanol were purchased from Lach-Ner, s.r.o., Czech Republic. Sodium carbonate (anhydrous) and sodium hydroxide were purchased from P-LAB, a.s., Czech Republic. Phosphate-buffered saline solution (PBS) was purchased from Lonza Biotec, s.r.o., Czech Republic. All chemicals were used as delivered.

The NO photodonor *N*-(3-aminopropyl)-3-(trifluoromethyl)-4-nitrobenzenamine (NOP) was synthesized and characterized according to the literature.[28] Briefly, 1.7 mL of 1,3-propyldiamine and 2.12 g of Na_2CO_3 were refluxed in 50 mL of EtOH for 15 min. Approximately 600 μL of 4-chloro-2-(trifluoromethyl)-1-nitrobenzene was added, and the mixture was continuously stirred for 3 days. After cooling to ambient temperature, the resulting suspension was filtered. The organic solution was concentrated under reduced pressure and purified by column chromatography (SiO_2, methanol 100%) to produce NOP as a yellow powder.

Electrospinning. A mixture of 0.07 wt % TEAB and 99.93 wt % PS was dissolved in cyclohexanone to prepare a 17% solution for the fabrication of the PS nanofiber material. The nanofiber materials were produced using the modified Nanospider electrospinning industrial technology.[6] This method used the simultaneous formation of charged liquid jets on the surface of a thin wire electrode in which the number and location of the jets is set up naturally in their optimal positions.[36] The diameters of the nanofibers were measured using the image analysis software, NIS Elements 4.0 (Laboratory Imaging, Czech Republic).

Ion-Exchange Capacity. Approximately 100 cm^2 of the sulfonated material was treated with 20 mL of a 10 mM NaOH solution for 1 day

DOI: 10.1021/acsami.5b06233
ACS Appl. Mater. Interfaces 2015, 7, 22980−22989

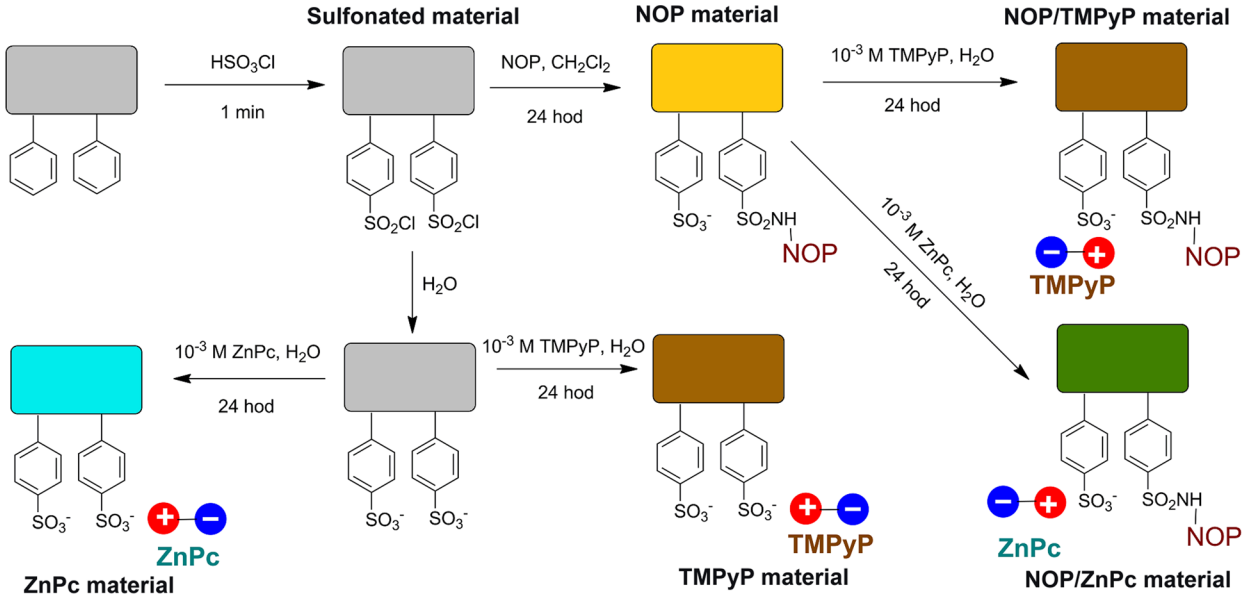

Figure 2. Schematic diagram of the preparation protocol for the photoactive nanofiber materials.

to exchange H^+ with Na^+. The remaining NaOH was titrated by 10 mM HCl using a potentiometric reading. The ion-exchange capacity (IEC) was related to the mass of the dried materials. The same procedure was also employed for the aminated materials. From the IEC, the quantity of the bonded compounds on the surface was calculated.

Scanning Electron Microscopy. The nanofiber morphology was studied using a scanning electron Quanta 200 FEG microscope (FEI, Czech Republic).

Contact Angle Measurements. The hydrophobic/hydrophilic character of the PS surfaces before and after functionalization was characterized by apparent contact angle (ACA) measurements using a Surface Energy Evaluation System (SEE System Standard, Czech Republic). The ACAs of the PS surfaces were measured using a 10 μL deionized water droplet. Each measurement was repeated three times to obtain an average value of the contact angle that was calculated by multipoint fitting of the drop profile using SEES software.

Fourier Transform Infrared Spectra. FTIR spectra were collected in the transmission mode using a Thermo Scientific FTIR spectrometer (Nicolet 6700) with Happ-Genzel apodization in the 400−4000 cm^{-1} range.

UV/Vis and Emission Spectroscopy. The UV/vis absorption spectra were recorded on a Varian 4000 spectrometer equipped with an integration sphere. The solutions were recorded in transmission mode. The sample of the nanofiber material (one layer on a quartz plate) was placed at the entrance of the sphere and measured in the diffuse reflectance mode to minimize light scattering. Steady-state emission spectra were recorded on an Aminco Bowman AB2 spectrometer.

Amperometric Detection of NO. The release of NO was measured with a World Precision Instrument ISO-NO meter equipped with a data acquisition system and was based on the direct amperometric detection of NO with a short response time (<5 s) and a sensitivity range of 1 nM to 20 μM. The analog signal was digitalized with a four-channel recording system and transferred to a computer. The sensor was accurately calibrated by mixing standard solutions of $NaNO_2$ with 0.1 M H_2SO_4 and 0.1 M KI according to the reaction:

$$4H^+ + 2I^- + 2NO_2^- \rightarrow 2H_2O + 2NO + I_2$$

A sample of the nanofiber material was fixed on a quartz plate and placed in a thermostatted quartz cell (1 × 1 × 3 cm^3) that was filled with H_2O. The irradiation was carried out using a 100 mW CW laser at 405 nm under continual stirring. The NO measurements were conducted using the electrode positioned outside the light path to avoid NO signal artifacts due to photoelectric interference on the ISO-NO electrode.

Chemical Detection of NO. The released NO was also detected using the DAN and myoglobin (Mb) chemical tests.[37,38] The DAN test is based on the reaction of nonfluorescent 2,3-diaminonaphthalene (DAN) with N_2O_3, which is immediately formed by reaction of NO with O_2. The reaction produces the highly fluorescent 2,3-naphthotriazole. A piece of the nanofiber material (2 cm^2 on a quartz plate) was placed in a thermostatted 10 mm quartz cell (22 °C) that contained 3.5 mL of 0.31 mM DAN in 0.62 M HCl. The cell was irradiated with visible light from a stabilized xenon lamp (500 W, Newport) with a long-pass filter ($\lambda \geq 400$ nm, Newport). After the irradiation, a 200 μL aliquot of the sample and 100 μL of 2.8 M NaOH were placed into a fluorescence detection cuvette and diluted with 3.2 mL of distilled H_2O. The NO was detected as emission at 450 nm (λ_{exc} = 365 nm).

The Mb test is based on the UV/vis detection of the $Mb(Fe^{II})$−NO adduct. The UV/vis spectra of 3.5 mL of 30 μM Mb in phosphate buffer (pH 7.0) before and after the addition of 250 μL of 0.05 M $Na_2S_2O_4$ in H_2O were recorded. The reduction of $Mb(Fe^{III})$ to $Mb(Fe^{II})$ was observed as a shift in the Soret band from 410 to 432 nm. A piece of the nanofiber material (2 cm^2 on a quartz plate) was added to the thermostatted 10 mm quartz cell (22 °C) that contained the freshly prepared $Mb(Fe^{II})$ detection solution. The cell was irradiated with visible light from a stabilized xenon lamp (500 W, Newport) with a long-pass filter ($\lambda \geq 400$ nm, Newport). After the irradiation, the Soret absorption band of the NO adduct at 420 nm was detected.

Time-Resolved Near-Infrared Luminescence of $O_2(^1\Delta_g)$. The material was placed on a quartz plate in oxygen- or argon-saturated D_2O. Alternatively, the samples that were wetted by D_2O were measured in an evacuated cell under an oxygen atmosphere or a vacuum. A Lambda Physik COMPEX102 excimer laser (308 nm, pulse width of 28 ns) and a FL 3002 dye laser (425 nm, 670 nm) were used for the excitation. The time-resolved near-infrared luminescence of $O_2(^1\Delta_g)$ at 1270 nm was observed at a right angle to the excitation pulse using a homemade detector unit (interference filter, Ge diode Judson J16-8SP-R05M-HS).

Photooxidation of Model Species by Nanofiber Materials. A piece of the nanofiber material was placed in a thermostatted 10 mm quartz cell (22 °C) that contained 2 × 10^{-4} M uric acid in 0.02 M phosphate buffer (pH 7.0) or a 0.1 M iodide detection solution. The cell was irradiated with visible light using a stabilized xenon lamp (500

DOI: 10.1021/acsami.5b06233
ACS Appl. Mater. Interfaces 2015, 7, 22980−22989

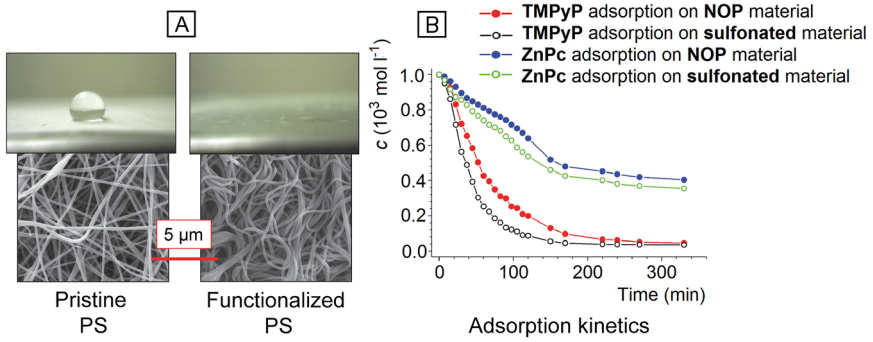

Figure 3. (A) Behavior of water droplet (top) and SEM image (bottom) of the pristine and functionalized nanofiber PS material (namely, **NOP** material). Similar SEM images and hydrophilic behavior were also found for **NOP/TMPyP** and **NOP/ZnPc** materials (Figure S1). (B) Kinetics of adsorption of 10^{-3} M TMPyP or 10^{-3} M ZnPc from aqueous solution (20 mL) to the sulfonated or **NOP** material (40 cm^2). The variable *c* designates the concentration of the TMPyP or ZnPc in the loading solution after immersion of the nanofiber material.

W, Newport) with a long-pass filter ($\lambda \geq 400$ nm, Newport). The UV absorbance changes at 292 nm (attributed to photodegradation of uric acid)[39] and at 287 or 351 nm (attributed to the formation of I_3^- in the iodide test)[40] were recorded at regular intervals and compared to those of a blank solution of the same composition that was stored in the dark.

Antibacterial Tests. For demonstration of antibacterial effect, a modified AATCC TM 100 test method was used. A culture of *Escherichia coli* DH5α (Invitrogen, CA, USA) that was resistant to ampicillin was incubated by stirring in LB medium that was enriched by ampicillin at 37 °C. The incubation was stopped when the absorbance at 560 nm reached a value of ca. 1. The prepared culture was diluted 10^4 times to the desired concentration in PBS. The nanofiber materials (5 cm^2, free or doped by the NO photodonor and photosensitizer) were placed in a quartz cuvette that contained 1.2 mL of the bacterial suspension, and they were then irradiated with visible light ($\lambda \geq 400$ nm) for 5 or 10 min or stored in the dark. After a brief shaking, 150 μL of the bacterial suspension was placed on the sterile agar plates. The plates were incubated for 16 h in the dark at 37 °C to allow the individual bacteria to grow and form colonies. The colony-forming units (CFU) were then counted.

For the demonstration of surface antibacterial effect, the surfaces of **NOP**, **NOP/TMPyP**, and **NOP/ZnPc** material were inoculated with 3 × 20 μL (approximately 6000 CFUs) of a suspension of *E. coli* in PBS. The samples were placed on agar plates at 5 °C (to hinder the fast evaporation of the bacterial suspension and escape of NO from the wet surface) and were either illuminated with white light for 5 or 10 min or were stored in the dark. Then, the samples were placed in Eppendorf tubes with 1 mL of PBS. After a brief shaking (2 × 3 s on an IKA Vortex 3), the PS nanofiber matrix was removed. Each bacterial suspension was centrifuged for 5 min at 3600 g. The supernatant (0.65 mL) was carefully removed. From the pellet media, 150 μL of each bacterial suspension was placed on sterile agar plates. The plates were incubated overnight in darkness at 37 °C to allow the individual bacteria to grow and form colonies.

RESULTS AND DISCUSSION

Preparation, Ion-Exchange Capacity, and Morphology of the Nanofiber Materials. The preparation of the individual nanofiber materials is depicted in Figure 2. The first steps were carried out in an air bag filled with nitrogen. The pristine electrospun PS nanofiber material (60 cm^2) was fixed on quartz substrates and immersed in a bath of 85 mL of HSO_3Cl for 1 min at ambient temperature. Then, the sulfonated material was washed with CH_2Cl_2 and immersed in 100 mL of a solution of 3 mM NOP in CH_2Cl_2 for 24 h. The material was removed from the air bag, washed with CH_2Cl_2, and allowed to dry in air (12 h) so that the unreacted $-SO_2Cl$ groups on the surface of the material were gently hydrolyzed to $-SO_3^-$ groups by the humidity in the air (**NOP** material).

The dry material was neutralized by 0.02 M phosphate buffer (pH 7.0), washed with H_2O, and placed into 20 mL of aqueous loading solution (10^{-3} M TMPyP or 10^{-3} M ZnPc) for 12 h. The free $-SO_3^-$ groups formed ion pairs with the tetracationic photosensitizers to produce **NOP/TMPyP** and **NOP/ZnPc** materials, respectively. Alternatively, the **TMPyP** and **ZnPc** materials were prepared by adsorption of 10^{-3} M TMPyP or 10^{-3} M ZnPc at the surface of the sulfonated pristine nanofiber materials. The concentrations of the photosensitizers can be easily followed spectroscopically and they were optimized in our previous study.[13]

Under controlled experimental conditions, NOP is unable to interact with all $-SO_2Cl$ groups. This allows the cationic photoactive photosensitizers to electrostatically bind to the remaining hydrolyzed anionic $-SO_3^-$ groups.

The sulfonation of the pristine material and the subsequent binding of the photoactive compounds slightly increase the average diameter of the PS nanofibers (Figure S1). Nevertheless, the nanofiber character of the material is still maintained even after the surface derivatization. The color changes caused by the surface modification are indications of the successful binding of the photoactive molecules: bright yellow for **NOP**, dark brown for **NOP/TMPyP**, and blue-green for **NOP/ZnPc** material (Figures 2 and S1).

In contrast to the pristine PS material, which is a hydrophobic material, **NOP**, **NOP/TMPyP**, and **NOP/ZnPc** materials are highly hydrophilic. The increased wettability can be characterized by the water droplet apparent contact angles. In fact, although the pristine material exhibited an apparent contact angle of 130 ± 4°, all of the **NOP**, **NOP/TMPyP**, and **NOP/ZnPc** materials are characterized by an apparent contact angle of ≤5° (Figure 3A). These hydrophilic features are important because it has been found that the increased wettability of the surface of a material which generates short-lived species with a short diffusion pathway (such as $O_2(^1\Delta_g)$) is a crucial factor for their efficient surface reaction with a substrate/biological target in an aqueous environment.[18]

A high ion-exchange capacity (IEC) of the chlorosulfonated and hydrolyzed PS nanofiber materials was observed (IEC = 2.5 mmol g^{-1}), in agreement with a previous study.[12] The IEC of **NOP** material is considerably suppressed by the bonding with NOP (IEC = 0.85 mmol g^{-1}). From the IEC difference (before and after the derivatization), we calculated that **NOP**, **NOP/TMPyP**, and **NOP/ZnPc** materials have a total of 1.65 mmol

DOI: 10.1021/acsami.5b06233
ACS Appl. Mater. Interfaces 2015, 7, 22980−22989

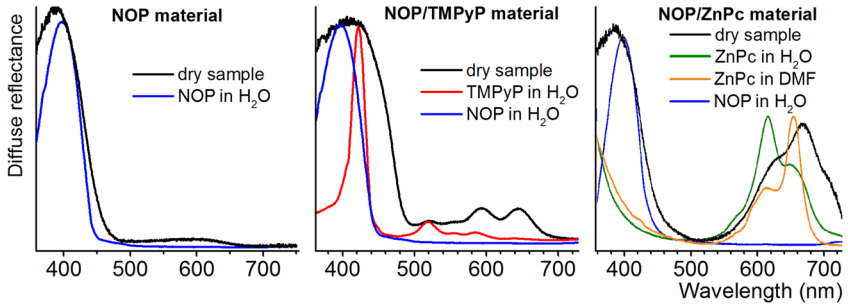

Figure 4. Normalized diffuse reflectance spectra of dry samples of **NOP**, **NOP/TMPyP**, and **NOP/ZnPc** materials compared with the absorption spectra of the corresponding photoactive compounds in H_2O or dimethylformamide.

g^{-1} (0.29 mg/cm^2) of NOP molecules bonded to the nanofibers.

Figure 3B shows the kinetics of the adsorption of 10^{-3} M TMPyP and 10^{-3} M ZnPc from aqueous solution to the surface of the sulfonated and **NOP** materials. The adsorption kinetics of the monomeric TMPyP is much faster than that of the ZnPc, which predominantly has a dimeric form in aqueous solution (Figure 4). The slow kinetics of adsorption of ZnPc can be attributed to the slow monomerization and/or reorganization of large ZnPc molecules on the surface of the nanofibers. The presence of NOP slightly decreases the adsorption kinetics of both TMPyP and ZnPc.

The analysis of the adsorption kinetics after 6 h of loading showed that **NOP/TMPyP** material had 0.75 mmol g^{-1} (0.68 mg TMPyP/cm^2) TMPyP bonded to the nanofiber material. The **NOP/ZnPc** material had 0.46 mmol g^{-1} (0.47 mg ZnPc/1 cm^2) ZnPc bonded to the nanofiber material. The ratio between the NO photodonors and the porphyrinoid photosensitizers bound to the nanofibers can be estimated to be ca. 2.2:1 and 3.6:1 for **NOP/TMPyP** and **NOP/ZnPc**, respectively. The materials are stable in the temperature range between 5 and 55 °C; the UV/vis spectra did not show any release of the photosensitizers into aqueous solutions.[41]

UV/Vis Spectra. Figure 4 shows the diffuse reflectance spectra of dry samples of **NOP**, **NOP/TMPyP**, and **NOP/ZnPc** materials and the corresponding spectra of the photoactive compounds in solution. The absorption band in the UV/vis spectrum of the bound **NOP** material appears at 387 nm, and it is blue-shifted by 13 nm compared with the corresponding band of free NOP (at 400 nm) in aqueous solution. Because this band is particularly sensitive to the solvent polarity, the blueshift can be attributed to the reduced polarity of the nanofiber material with respect to water and, analogously, to the same observed chromogenic center in other hydrophobic nanomaterials.[42]

The UV/vis spectrum of **NOP/TMPyP** material is characterized by the overlapping Soret band of the TMPyP (423 nm in aqueous solution) and absorption band of NOP. Nevertheless, the presence of the characteristic Q-bands of TMPyP in the red region serves as evidence of the surface modification by porphyrin.[12]

Additionally, the UV/vis spectrum of **NOP/ZnPc** material exhibits a representative band for NOP that partially overlaps with the Soret band of ZnPc in the blue region. In the red region, bands that are representative of the dimer and the prevailing monomer of ZnPc at 687 nm were observed. The bands are red-shifted by 10 nm with respect to those of the aqueous solution in which ZnPc exhibits absorption bands for its dimer at 630 nm and its monomer at 677 nm. The monomer form is predominant in less polar solvents, e.g., in dimethylformamide. Figure 4 indicates that the dimerization of ZnPc that is found in aqueous solution even at low concentration (10^{-6} M) is considerably reduced after binding to the nanofiber material. This fact is important because dimerization or higher aggregation, typical features of phthalocyanines, generally significantly quenches the excited states and decreases the photoactivity of phthalocyanines.[43]

FTIR spectra. The prepared nanofiber materials were characterized by FTIR (Figure 5). The spectra were compared with those of pristine and sulfonated nanofiber materials and the spectra of the individual photoactive compounds, i.e., NOP, TMPyP, and ZnPc.

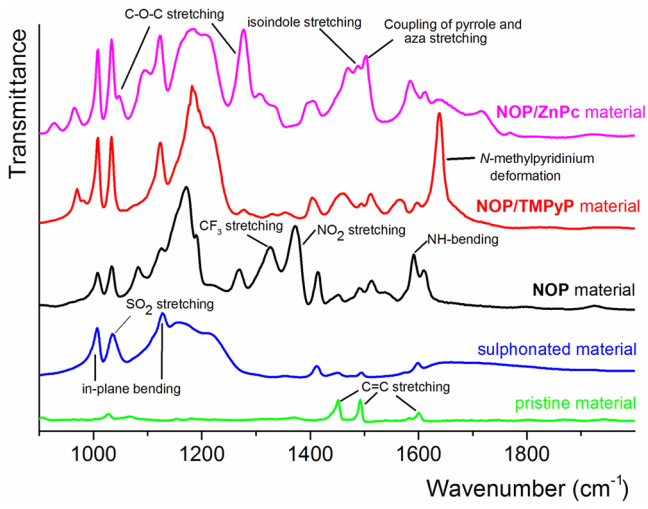

Figure 5. FTIR spectra of the individual nanofiber materials.

The pristine electrospun material exhibits main absorption bands at 1600, 1492, and 1451 cm^{-1} (C═C aromatic stretching) and 1028 cm^{-1} (C−H in-plane bending). Sulfonation of the material resulted in a strong band at 1036 cm^{-1} and a doublet at 1210 and 1160 cm^{-1}, which correspond to the symmetric and asymmetric SO_2 stretching vibrations, respectively. The bands at 1127 and 1006 cm^{-1} are assigned to the in-plane bending of the para-substituted phenyl ring, which confirms the successful sulfonation of the nanofiber.[44] Amination of PS is confirmed by the appearance of three characteristic bands at 1326 cm^{-1} (CF_3 stretching vibration), 1372 cm^{-1} (NO_2 stretching vibration), and 1590 cm^{-1} (N−H bending vibration) in the spectrum of **NOP** material. Moreover, the N−H bonds exhibit a wide intensive band at approximately 3400 cm^{-1} (not shown in Figure 5) that is also

DOI: 10.1021/acsami.5b06233
ACS Appl. Mater. Interfaces 2015, 7, 22980−22989

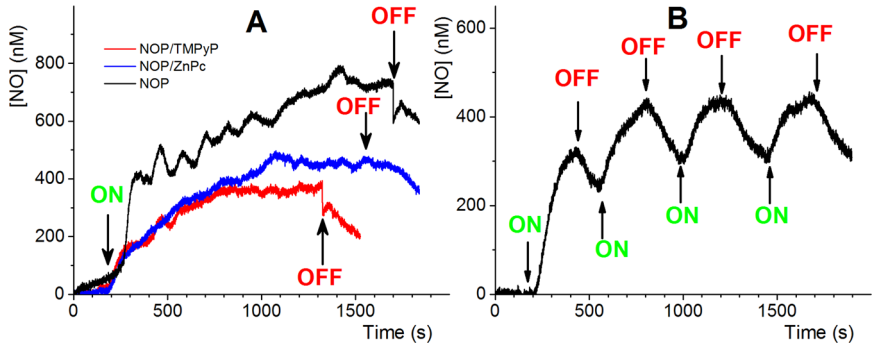

Figure 6. (A) Amperometric detection of the NO photoreleased from the surface of **NOP** (black trace), **NOP/TMPyP** (red trace), and **NOP/ZnPc** (blue trace) materials. The arrows indicate the switch-on and switch-off character of the NO release that was triggered by the irradiation (λ_{exc} = 405 nm). (B) NO release profile observed upon alternate period of illumination of **NOP** material.

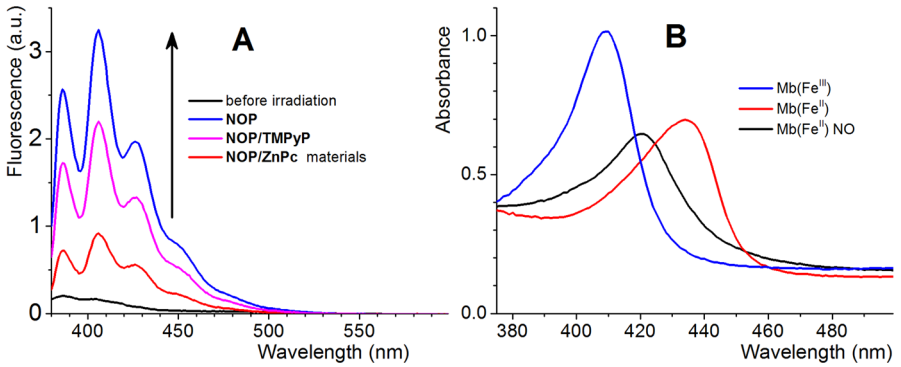

Figure 7. (A) Fluorescence detection of the photorelease of NO from the surface of **NOP**, **NOP/TMPyP**, and **NOP/ZnPc** materials via the DAN method. The fluorescence (λ_{exc} = 365 nm) of 3.5 mL of 0.31 mM DAN in 0.62 M HCl with the nanofiber material (8 cm^2) before and after 50 min of irradiation (indicated by arrow) with visible light. (B) Myoglobin test for detection of the NO released from the surface of **NOP/TMPyP** material after 2 min of irradiation by visible light. Mb(Fe^{III}) (3 mM in 0.02 M phosphate buffer, pH 7.0), black trace; its reduced form Mb(Fe^{II}) before and after binding of the released NO, red and blue traces, respectively.

present in the FTIR spectra of **NOP/TMPyP** and **NOP/ZnPc** materials. The narrow band from the deformation vibration of the *N*-methylpyridinium group at 1638 cm^{-1} dominates the FTIR spectra of **NOP/TMPyP** material, and it overlaps with the N−H bending band.[45] However, the binding of ZnPc is clearly confirmed in the spectrum of **NOP/ZnPc** material by the appearance of a band at 1502 cm^{-1} that corresponds to the coupling of pyrrole and aza stretching. The adjacent band at 1489 cm^{-1} is caused by an isoindole stretching vibration. The asymmetric stretching of the C−O−C bonds that connect the methoxypyridinium groups to the phthalocyanine skeleton appears as a strong band at 1277 cm^{-1}. The symmetrical stretching of this bond shows a small peak at 1048 cm^{-1}, which is almost overlapped by the strong absorption of the $-SO_3^-$ group.[46]

NO Photorelease. All of the prepared **NOP**, **NOP/TMPyP**, and **NOP/ZnPc** materials release NO from the surface when irradiated by visible light. Figure 6A illustrates the release of NO from all materials immersed in H_2O, as monitored by the amperometric method,[47] which allows the direct detection and quantification of this radical species. The switch-on/switch-off cycling of the excitation laser demonstrates a stable and controllable NO release that is exclusively regulated by light excitation (Figure 6B). The NO release is accompanied by a delay in the electrode response, which can be attributed to the time necessary for diffusion of the photoreleased NO from the nanofiber to the electrode. The sharp increase of the NO release at the beginning of the irradiation is probably due to the high amount of photons absorbed by the NO photodonor alone in the initial stage of the photoreaction. As the irradiation time increases, the rate of the NO photorelease decreases, according to the lower concentration of the NO photodonors resulting from the photodecomposition of this precursor.

In addition to amperometric detection, other chemical methods were employed to determine the propensity of the new materials to photorelease NO under physiological conditions. The DAN assay is one of the most sensitive and selective fluorescence-based methods for NO detection.[37] As is evident from Figures 6A and 7A, under the same experimental conditions the greatest amount of photoreleased NO was observed for **NOP** material. The lower amount of NO photoreleased from the surface of **NOP/ZnPc** and especially **NOP/TMPyP** materials (Figure 7A) can be attributed to the filter effect of the bound photosensitizer. The Soret band of TMPyP in **NOP/TMPyP** material overlaps with the absorption band of NOP, which leads to less NO release. The reduced overlap of the absorption bands of ZnPc and NOP in the blue region also causes a decrease in the NO production, but this effect is lower.

The photoreleased NO from the surfaces of **NOP**, **NOP/TMPyP**, and **NOP/ZnPc** materials was also followed with the myoglobin test. Analogous to other heme proteins, equine skeletal myoglobin (Mb) binds NO via its metal center.[48] The binding to Mb of NO photoreleased from the nanofiber materials was observed in the absorption spectra of Mb (Figure

DOI: 10.1021/acsami.5b06233
ACS Appl. Mater. Interfaces 2015, 7, 22980−22989

7B). The appearance of a Soret band at 420 nm confirmed the binding of NO to the Fe(II) of the heme group of Mb.[38] Control experiments carried out for the irradiated solutions that contained reduced Mb in the absence of **NOP**, **NOP/TMPyP**, or **NOP/ZnPc** or in the presence of **NOP**-free nanofiber material did not result in the formation of the adduct.

$O_2(^1\Delta_g)$ Photorelease. Singlet oxygen, $O_2(^1\Delta_g)$, was formed via intersystem crossing from the photoexcited triplet states of the photosensitizers.[49] The kinetics of $O_2(^1\Delta_g)$ was followed by time-resolved near-infrared luminescence. The luminescence of $O_2(^1\Delta_g)$ of the dry samples or samples immersed in H_2O was below the detection limit of our setup. This may be due to the aggregation of the photosensitizers in the dry sample[13] or to the low lifetime of $O_2(^1\Delta_g)$ in H_2O (3.5 μs).[15] The luminescence was measured with samples immersed to D_2O, where the lifetime of $O_2(^1\Delta_g)$ diffused from photosensitizer, τ_Δ, is more than 1 order of magnitude higher than that of H_2O,[16] and it was calculated as the difference between the sample signals immersed in oxygen- and argon-saturated solvent (Figure 8). The initial part of the signals (0−5 μs) can fail because of strong prompt fluorescence of the photosensitizer and saturation of the detector.

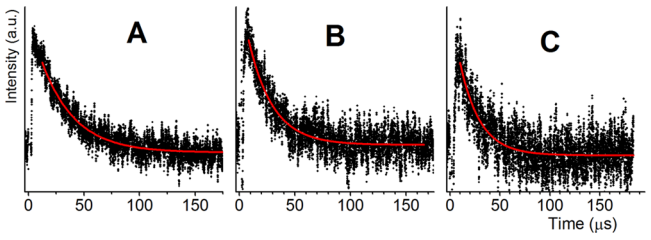

Figure 8. Luminescence intensity of $O_2(^1\Delta_g)$ after excitation of (A) **NOP/TMpyP** material (λ_{exc} = 308 nm), (B) **NOP/ZnPc** material (λ_{exc} = 670 nm), and (C) **ZnPc** (λ_{exc} = 670 nm) material with 670 nm. The solid red lines represent a single exponential fit of the experimental data (eq 1).

The resulting kinetics of $O_2(^1\Delta_g)$ was monoexponential (Figure 8) and can be described using eq 1, which is valid for $\tau_\Delta \gg \tau_T$:[13]

$$I = I_0 \exp(-t/\tau_\Delta) \quad (1)$$

where τ_T is the lifetime of the photosensitizer triplet states, τ_Δ is the corresponding lifetime of $O_2(^1\Delta_g)$, and I and I_0 denote the luminescence intensity of $O_2(^1\Delta_g)$ at time t and after excitation (t = 0), respectively.

The calculated $\tau_\Delta = 29 \pm 2$ μs for **NOP/TMPyP** and $\tau_\Delta = 21 \pm 2$ μs for **NOP/ZnPc** material from five independent measurements of different samples of the same materials are longer than previously published data for nanofiber material that has ionically attached TMPyP on the surface of sulfonated nanofibers.[13] It indicates suppressed quenching of $O_2(^1\Delta_g)$ by the surroundings.

The amount and ratio of NO and $O_2(^1\Delta_g)$ that is released from the nanofiber materials can be tuned by the selection of the irradiation wavelength. Both species are released simultaneously from **NOP/TMPyP** material upon excitation with the blue part of visible light (Figures 6, 7, and 8A) because of the overlap of the strong absorption band of NOP and the Soret band of TMPyP (Figure 4). However, the selective photoexcitation of ZnPc in the **NOP/ZnPc** material by red light (strong Q-band of ZnPc at 670 nm) allows efficient formation of $O_2(^1\Delta_g)$ (Figure 8B) and suppresses the production of NO (Figure 4). We did not observe any quenching of $O_2(^1\Delta_g)$ by the covalently bonded NOP because the lifetime of $O_2(^1\Delta_g)$ ($\tau_\Delta = 22 \pm 1$ μs) that is photogenerated from the **ZnPc** material (Figure 8C) corresponds with $\tau_\Delta = 21 \pm 2$ μs for **NOP/ZnPc** material.

Although the direct observation of the time-resolved phosphorescence of $O_2(^1\Delta_g)$ confirmed the photogeneration of $O_2(^1\Delta_g)$, its oxidation ability in an aqueous environment was confirmed by two chemical methods: iodide detection[40] and photobleaching of uric acid.[39] As an example, the continuous irradiation of **NOP/TMPyP** material in aerated aqueous solutions of I^- was accompanied by a linear increase of the I_3^- concentration in the solution (proportional to photogeneration of $O_2(^1\Delta_g)$) (Figure 9A). The presence of NaN_3, a known physical quencher of $O_2(^1\Delta_g)$, efficiently inhibited the photooxidation of the I^- substrate (Figure 9B). UV/vis spectra of the nanofiber materials measured before and after the irradiation revealed no changes in the Soret and Q-bands of the TMPyP and ZnPc photosensitizers, which indicates high stability of the materials.

Antibacterial Activity. The antibacterial properties of nanofiber materials with ionically attached or encapsulated photosensitizers and their strong bacterial inhibition on the surface has been extensively studied in our laboratory.[6−10,13,17,18] According to our previous studies, we found a surface antibacterial effect toward *E. coli* for all **NOP**, **NOP/TMPyP**, and **NOP/ZnPc** materials. Evidently, not only materials photogenerating $O_2(^1\Delta_g)$ but also materials releasing NO alone can ensure antibacterial surface after irradiation by visible light (Figure 10A).

Nevertheless, the NO generated from the surface of the nanofiber materials with longer lifetimes up to a few seconds depending on oxygen concentration[23,50] and consequently longer diffusion pathways can cause the sterilization of a large area in comparison with nanomaterials that photogenerate only $O_2(^1\Delta_g)$ with a short lifetime and diffusion pathway. To confirm this, the following antibacterial experiment was carried out. The **NOP**, **NOP/TMPyP**, and **NOP/ZnPc** materials were immersed in suspensions of *E. coli* and irradiated or kept in the dark. Then, an aliquot of the treated bacterial suspension was placed on an agar plate and incubated overnight (Figure S2). Figures 10B and S2 illustrate strong bacterial growth inhibition of *E. coli* in space after 5 and 10 min of irradiation with visible light for a bacterial suspension in the presence of NOP. Similar observations were found for **NOP/TMPyP** and **NOP/ZnPc** materials. The slight reduction in the antibacterial effect can be attributed to the shielding effect, which lowers the amount of photoreleased NO (Figure 6). **NOP**, **NOP/TMPyP**, and **NOP/ZnPc** materials that were kept in the dark did not exhibit any bacterial inhibition compared with the effect of sulfonated material that did not contain the photoactive compounds.

Minor antibacterial effects can be attributed to the light itself (irradiated/nonirradiated sulfonated material). The irradiated **TMPyP** or **ZnPc** materials that have only ionically bonded photosensitizers exhibited an insignificant level of bacterial inhibition (compared with that of the irradiated sulfonated control) in suspension because of the short lifetime and pathway of $O_2(^1\Delta_g)$, which enables the antibacterial effect over a short distance. Briefly, only the presence of the NO photodonor bound to the nanofiber materials (**NOP**, **NOP/**

DOI: 10.1021/acsami.5b06233
ACS Appl. Mater. Interfaces 2015, 7, 22980−22989

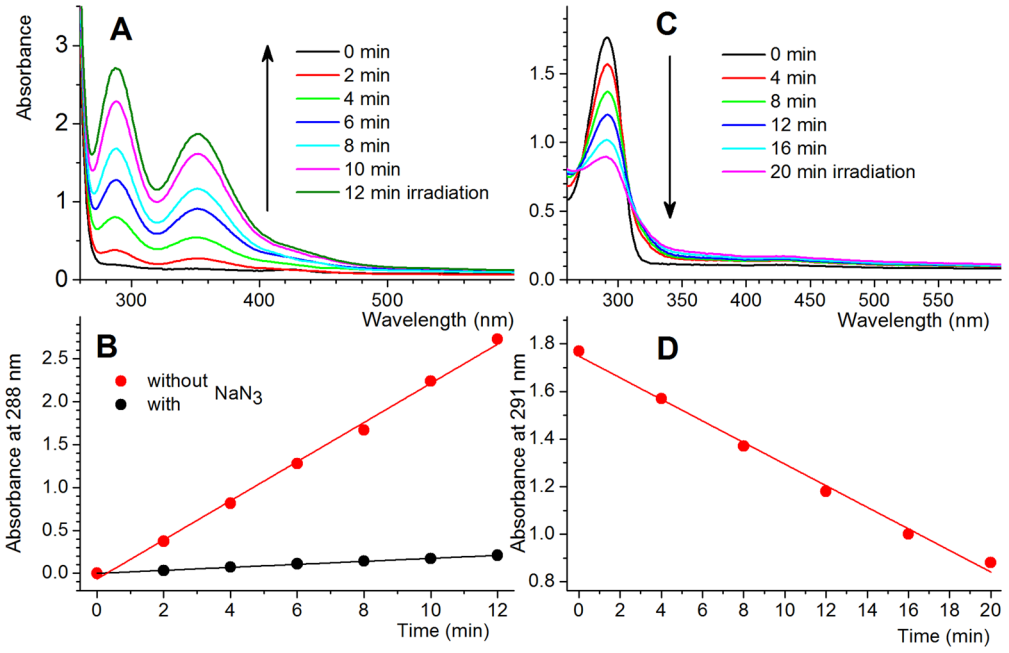

Figure 9. (A) Absorption changes of 3 mL of an air-saturated aqueous solution of 0.1 M I^- containing 3 cm^2 of **NOP/TMPyP** material during continuous irradiation with visible light at 22 °C. (B) Time course of the photogeneration of I_3^- monitored at 287 nm in H_2O and in the presence of 0.1 M NaN_3. (C) Changes in the absorption spectrum and (D) the absorbance at 292 nm of 3 mL of air-saturated 2×10^{-4} mol L^{-1} uric acid in 0.02 mol L^{-1} phosphate buffer (pH 7.0) that contained 3 cm^2 of **NOP/TMPyP** material during continuous irradiation with visible light. The arrows indicate the course of the photooxidation.

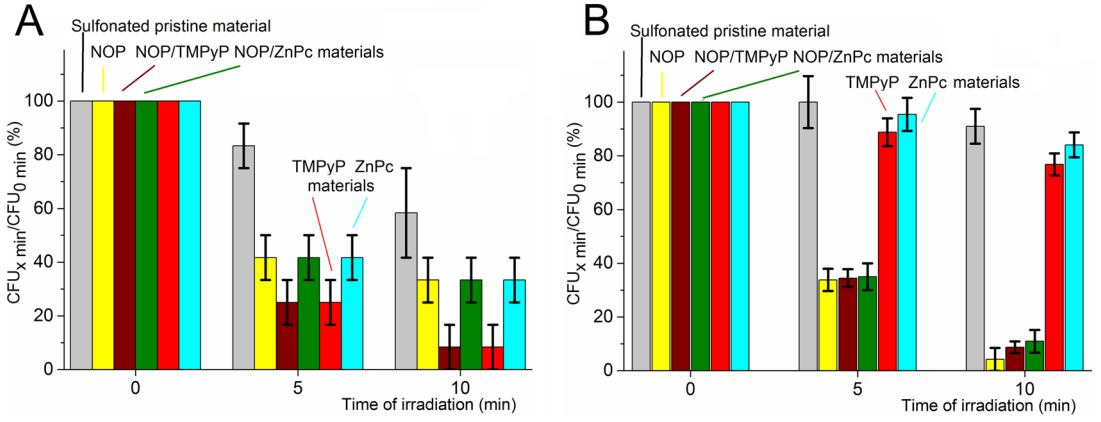

Figure 10. (A) Surface photoantibacterial activity of **NOP**, **NOP/TMPyP**, **NOP/ZnPc**, **TMPyP** and **ZnPc** materials compared with that of sulfonated pristine nanofiber material. (B) Space photoantibacterial activity of **NOP**, **NOP/TMPyP**, **NOP/ZnPc**, **TMPyP** and **ZnPc** materials compared with that of sulfonated pristine nanofiber material immersed in a suspension of *E. coli*. The results show the estimated average ratio of the CFUs observed on the agar plates for the irradiated (5 and 10 min) versus nonirradiated samples from three independent tests.

TMPyP, and **NOP/ZnPc**) exhibited an efficient antibacterial effect due to the formation of the long-lived NO.

The high surface area and the nanoporous structure of nanofiber material modified by combination of two types of photoactive compounds offer the great advantage of providing a high concentration of photoactive compounds and preventing bacteria and other pathogens from passing through the nanofiber materials. The bacteria and other pathogens are detained on the surface and killed by the photogenerated NO, $O_2(^1\Delta_g)$, or both.

NO-photoreleasing materials cannot ensure long-time antibacterial action. In fact, in contrast to the photogeneration of $O_2(^1\Delta_g)$, NO photoproduction is not a photocatalytic process because the amount of released NO is strictly limited by the reservoir of NOP on the nanofiber materials. Nevertheless, the nanofiber materials that contain NOP in combination with the photosensitizers evidently increase the antibacterial range and the possible usefulness of the nanofiber materials (doped only by photosensitizers) for medical applications, e.g., for covering/healing of chronic wounds. They also offer four important functionalities: (i) the ability to detain bacteria and other pathogens on the nanoporous surface, (ii) a sterile character, which is produced by the antibacterial NO and $O_2(^1\Delta_g)$ species generated on the surface with increased wettability, (iii) the antibacterial action due to the photoreleased NO, and (iv) the vasodilation effect that is caused by NO. Another intriguing advantage of combining NO with $O_2(^1\Delta_g)$ is related to the oxygen-independent antibacterial activity of NO. This may well complement the antibacterial

DOI: 10.1021/acsami.5b06233
ACS Appl. Mater. Interfaces 2015, 7, 22980−22989

action induced by $O_2(^1\Delta_g)$ under hypoxic conditions where photodynamic activity may fail.

CONCLUSIONS

We have reported a simple method for the preparation and postprocessing modification of electrospun polystyrene nanofiber materials with a covalently bound NO photodonor and ionically entangled tetracationic TMPyP or ZnPc photosensitizers on the surface. These photoactivated multifunctional nanofiber materials simultaneously generate two small antibacterial species, $O_2(^1\Delta_g)$, with a short radius of antibacterial action, and NO, with a long radius of antibacterial action, under the exclusive control of visible light. The dual-mode photoantibacterial action observed under the daylight illumination in combination with the nanoporous character of the material detaining pathogens, such as bacteria, on its surface make the engineered nanofibers intriguing systems for any application where a sterile environment has to be introduced and/or maintained. Considering the industrial scale of the electrospinning process, the presented nanofiber materials have a great potential to address various medical-, biological-, and environmental-related issues.

ASSOCIATED CONTENT

Supporting Information

The Supporting Information is available free of charge on the ACS Publications website at DOI: 10.1021/acsami.5b06233.

Photographs and SEM images of the nanofiber material samples, photographs of the bacterial colonies illustrating the antibacterial effect, and a table with CFU that documents the antibacterial effect of the nanofiber materials.
(PDF)

AUTHOR INFORMATION

Corresponding Authors

*E-mail: ssortino@unict.it.
*E-mail: mosinger@natur.cuni.cz.

Notes

The authors declare no competing financial interest.

ACKNOWLEDGMENTS

This work was supported by the Czech Science Foundation (13-12496S). We also thank the Marie Curie Program (FP7-PEOPLE-ITN-2013, CYCLON-HIT 608407) and the MIUR (PRIN 2011) for financial support. We thank Dr. Lukáš Plíštil for preparation of the nanofiber materials via electrospinning.

ABBREVIATIONS

NOP = N-(3-aminopropyl)-3-(trifluoromethyl)-4-nitrobenzenamine
TMPyP = 5,10,15,20-tetrakis (*N*-methylpyridinium-4-yl)-porphyrin
ZnPc = zinc(II) 2,9,16,23-tetrakis(*N*-methyl-pyridiumoxy) phthalocyanine
NOP material = nanofiber material with covalently bound NOP
NOP/TMPyP material = nanofiber material with covalently bound NOP and ionically bound TMPyP
NOP/ZnPc material = nanofiber material with covalently bound NOP and ionically bound ZnPc
TMPyP material = nanofiber material with ionically bound TMPyP
ZnPc material = nanofiber material with ionically bound ZnPc

REFERENCES

(1) Greiner, A.; Wendorff, J. H. Electrospinning: A Fascinating Method for the Preparation of Ultrathin Fibers. *Angew. Chem., Int. Ed.* **2007**, *46*, 5670−5703.
(2) Li, W. J.; Laurencin, C. T.; Caterson, E. J.; Tuan, R. S.; Ko, F. K. Electrospun Nanofibrous Structure: A Novel Scaffold for Tissue Engineering. *J. Biomed. Mater. Res.* **2002**, *60*, 613−621.
(3) Ma, Z. V.; Kotaki, M.; Ramakrishna, S. Surface Modified Nonwoven Polysulphone (PSU) Fiber Mesh by Electrospinning: A Novel Affinity Membrane. *J. Membr. Sci.* **2006**, *272*, 179−187.
(4) Martins, A.; Chung, S.; Pedro, A. J.; Sousa, R. A.; Marques, A. P.; Reis, R. L.; Neves, N. M. Hierarchical Starch-Based Fibrous Scaffolds for Bone Tissue Engineering Applications. *J. Tissue Eng. Regener. Med.* **2009**, *3*, 37−42.
(5) Yoo, H. S.; Kim, T. G.; Park, T. G. Surface-Functionalized Electrospun Nanofibers for Tissue Engineering and Drug Delivery. *Adv. Drug Delivery Rev.* **2009**, *61*, 1033−1042.
(6) Mosinger, J.; Jirsák, O.; Kubát, P.; Lang, K.; Mosinger, B. Bactericidal Nanofabrics Based on Photoproduction of Singlet Oxygen. *J. Mater. Chem.* **2007**, *17*, 164−166.
(7) Mosinger, J.; Lang, K.; Kubát, P.; Sýkora, J.; Hof, M.; Plíštil, L.; Mosinger, B. Photofunctional Polyurethane Nanofabrics Doped by Zinc Tetraphenylporphyrin and Zinc Phthalocyanine Photosensitizers. *J. Fluoresc.* **2009**, *19*, 705−713.
(8) Jesenská, S.; Plíštil, L.; Kubát, P.; Lang, K.; Brožová, L.; Popelka, Š.; Szatmáry, L.; Mosinger, J. Antibacterial Nanofiber Materials Activated by Light. *J. Biomed. Mater. Res., Part A* **2011**, *99A*, 676−683.
(9) Arenbergerová, M.; Arenberger, P.; Bednář, M.; Kubát, P.; Mosinger, J. Light-Activated Nanofibre Textiles Exert Antibacterial Effects in the Setting of Chronic Wound Healing. *Exp. Dermatol.* **2012**, *21*, 619−624.
(10) Lhotáková, Y.; Plíštil, L.; Morávková, A.; Kubát, P.; Lang, K.; Forstová, J.; Mosinger, J. Virucidal Nanofiber Textiles Based on Photosensitized Production of Singlet Oxygen. *PLoS One* **2012**, *7*, e49226.
(11) Reneker, D. H.; Chun, I. Nanometre Diameter Fibres of Polymer, Produced by Electrospinning. *Nanotechnology* **1996**, *7*, 216−223.
(12) Liu, X.; Lin, T.; Fang, J.; Yao, G.; Zhao, H.; Dodson, M.; Wang, X. In Vivo Wound Healing and Antibacterial Performances of Electrospun Nanofibre Membranes. *J. Biomed. Mater. Res., Part A* **2010**, *94A*, 499−508.
(13) Henke, P.; Lang, K.; Kubát, P.; Sýkora, J.; Šlouf, M.; Mosinger, J. Polystyrene Nanofiber Materials Modified with an Externally Bound Porphyrin Photosensitizer. *ACS Appl. Mater. Interfaces* **2013**, *5*, 3776−3783.
(14) Mosinger, J.; Lang, K.; Plíštil, L.; Jesenská, S.; Hostomský, J.; Zelinger, Z.; Kubát, P. Fluorescent Polyurethane Nanofabrics: A Source of Singlet Oxygen and Oxygen Sensing. *Langmuir* **2010**, *26*, 10050−10056.
(15) Hatz, S.; Poulsen, L.; Ogilby, P. R. Time-resolved Singlet Oxygen Phosphorescence Measurements from Photosensitized Experiments in Single Cells: Effects of Oxygen Diffusion and Oxygen Concentration. *Photochem. Photobiol.* **2008**, *84*, 1284−1290.
(16) Wilkinson, F.; Helman, W. P.; Ross, A. B. Rate Constants for the Decay and Reactions of the Lowest Electronically Excited Singlet State of Molecular Oxygen in Solution. An Expanded and Revised Compilation. *J. Phys. Chem. Ref. Data* **1995**, *24*, 663−677.
(17) Plíštil, L.; Henke, P.; Kubát, P.; Mosinger, J. Anion Exchange Nanofiber Materials Activated by Daylight with a Dual Antibacterial Effect. *Photochem.Photobiol.Sci.* **2014**, *13*, 1321−1329.
(18) Henke, P.; Kozak, H.; Artemenko, A.; Kubát, P.; Forstová, J.; Mosinger, J. Superhydrophylic Polystyrene Nanofiber Material

DOI: 10.1021/acsami.5b06233
ACS Appl. Mater. Interfaces 2015, 7, 22980−22989

Generating $O_2(^1\Delta_g)$: Postprocessing Surface Modification Toward Efficient Antibacterial Effect. *ACS Appl. Mater. Interfaces* **2014**, *6*, 13007−13014.
(19) Fang, F. G. *Nitric Oxide and Infections*; Kluwer Academic/Plenum Publishers; New York, 1999.
(20) Wang, P. G.; Xian, M.; Tang, X.; Wu, X.; Wen, Z.; Cai, T.; Janczuk, A. J. Nitric Oxide Donors: Chemical Activities and Biological Applications. *Chem. Rev.* **2002**, *102* (4), 1091−1134.
(21) Feelisch, M.; Stamler, J. S. Donors of Nitrogen Oxides. In *Methods in Nitric Oxide Research*; Feelisch, M., Stamler, J. S., Eds.; John Wiley & Sons: New York, 1996; pp 71−115.
(22) Rose, M. J.; Mascharak, P. K. Photoactive Ruthenium Nitrosyls: Effects of Light and Potential Application as NO Donors. *Coord. Chem. Rev.* **2008**, *252*, 2093−2114.
(23) Sortino, S. Light-Controlled Nitric Oxide Delivering Molecular Assemblies. *Chem. Soc. Rev.* **2010**, *39*, 2903−2913.
(24) Ford, P. C. Photochemical Delivery of Nitric Oxide. *Nitric Oxide* **2013**, *34*, 56−64.
(25) Seabra, A. B.; Duran, N. Nitric Oxide-Releasing Vehicles for Biomedical Applications. *J. Mater. Chem.* **2010**, *20*, 1624−1637.
(26) Sortino, S. Photoactivated Nanomaterials for Biomedical Release Applications. *J. Mater. Chem.* **2012**, *22*, 301−318.
(27) Wold, K. A.; Damodaran, V. B.; Suazo, L. A.; Bowen, R. A.; Reynolds, M. M. Fabrication of Biodegradable Polymeric Nanofibers with Covalently Attached NO Donors. *ACS Appl. Mater. Interfaces* **2012**, *4*, 3022−3030.
(28) Callari, F. L.; Sortino, S. Amplified Nitric Oxide Photorelease in DNA Proximity. *Chem. Commun.* **2008**, 1971−1973.
(29) Villanueva, A.; Caggiari, L.; Jori, G.; Milanesi, C. Morphological Aspects of an Experimental Tumour Photosensitized with a Meso-Substituted Cationic Porphyrin. *J. Photochem. Photobiol., B* **1994**, *23*, 49−56.
(30) Černý, J.; Karásková, M.; Rakušan, J.; Nešpůrek, S. Reactive Oxygen Species Produced by Irradiation of some Phthalocyanine Derivatives. *J. Photochem. Photobiol., A* **2010**, *210*, 82−88.
(31) Fraix, A.; Kandoth, N.; Sortino, S. Nitric Oxide Photoreleasing Nanoconstructs with Multiple Photofunctionalities. *Specialist Periodical Reports in Photochemistry* **2013**, *41*, 302−318.
(32) Vittorino, E.; Giancane, G.; Bettini, S.; Valli, L.; Sortino, S. Dual Funtion Multilayers for the Photodelivery of Nitric Oxide and Singlet Oxygen. *J. Mater. Chem.* **2009**, *19*, 8253−8258.
(33) Fraix, A.; Manet, I.; Ballestri, M.; Guerrini, A.; Dambruoso, P.; Sotgiu, G.; Varchi, G.; Camerin, M.; Coppellotti, O.; Sortino, S. Polymer Nanoparticles with Electrostatically Loaded Multicargo for Combined Cancer Phototherapy. *J. Mater. Chem. B* **2015**, *3*, 3001−3010.
(34) Fraix, A.; Kandoth, N.; Manet, I.; Cardile, V.; Graziano, A. C. E.; Gref, R.; Sortino, S. An Engineered Nanoplatform for Bimodal Anticancer Phototherapy with Dual-Color Fluorescence Detection of Sensitizers. *Chem. Commun.* **2013**, *49*, 4459−4461.
(35) Kandoth, N.; Kirejev, V.; Monti, S.; Gref, R.; Ericson, M. B.; Sortino, S. Two-Photon-Fluorescence Imaging and Bimodal Phototherapy of Epidermal Cancer Cells with Biocompatible Self-Assembled Polymer Nanoparticles. *Biomacromolecules* **2014**, *15*, 1768−1776.
(36) Forward, K. M.; Rutledge, G. C. Free Surface Electrospinning from a Wire Electrode. *Chem. Eng. J.* **2012**, *183*, 492−503.
(37) Carré, M. C.; Mahieuxe, B.; André, J. C.; Viriot, M. L. Fluorimetric Nitrite Analysis Using 2,3-diaminonaphthalene: An Improvement of the Method. *Analusis* **1999**, *27*, 835−838.
(38) Romberg, R. W.; Kassner, R. J. Nitric Oxide and Carbon Monoxide Equilibria of Horse Myoglobin and (*N*-methylimidazole)-protoheme. Evidence for Steric Interaction with the Distal Residues. *Biochemistry* **1979**, *18*, 5387−5392.
(39) Fischer, F.; Graschew, G.; Sinn, H. J.; Maier-Borst, W.; Lorenz, W. J.; Schlag, P. M. A Chemical Dosimeter for the Determination of the Photodynamic Activity of Photosensitizers. *Clin. Chim. Acta* **1998**, *274* (1), 89−104.
(40) Mosinger, J.; Mosinger, B. Photodynamic Sensitizers Assay: Rapid and Sensitive Iodometric Measurement. *Experientia* **1995**, *51*, 106−109.
(41) Suchánek, J.; Henke, P.; Mosinger, J.; Zelinger, Z.; Kubát, P. Effect of Temperature on Photophysical Properties of Polymeric Nanofiber Materials with Porphyrin Photosensitizers. *J. Phys. Chem. B* **2014**, *118*, 6167−6174.
(42) Kandoth, N.; Mosinger, J.; Gref, R.; Sortino, S. A NO Photoreleasing Supramolecular Hydrogel with Bactericidal Action. *J. Mater. Chem. B* **2013**, *1*, 3458−3463.
(43) Maya, E. M.; Snow, A. W.; Shirk, J. S.; Pong, R. G. S.; Flom, S. R.; Roberts, G. L. Synthesis, Aggregation Behavior and Nonlinear Absorption Properties of Lead Phthalocyanines Substituted with Siloxane Chains. *J. Mater. Chem.* **2003**, *13*, 1603−1613.
(44) Atorngitjawat, P.; Runt, J. Dynamics of Sulfonated Polystyrene Ionomers Using Broadband Dielectric Spectroscopy. *Macromolecules* **2007**, *40*, 991−996.
(45) de Miguel, G.; Perez-Morales, M.; Martin-Romero, M. T.; Munoz, E.; Richardson, T. H.; Camacho, L. J-Aggregation of a Water-Soluble Tetracationic Porphyrin in Mixed LB Films with a Calix[8]arene Carboxylic Acid Derivative. *Langmuir* **2007**, *23*, 3794−3801.
(46) Bao, M.; Pan, N.; Ma, C.; Arnold, D. P.; Jiang, J. Infrared Spectra of Phthalocyanine and Naphthalocyanine in Sandwich-Type (Na)phthalocyaninato and Porphyrinato Rare Earth Complexes - Part 4. The Infrared Characteristics of Phthalocyanine in Heteroleptic Tris(phthalocyaninato) Rare Earth Complexes. *Vib. Spectrosc.* **2003**, *32*, 175−184.
(47) Coneski, P. N.; Schoenfisch, M. H. Nitric Oxide Release: Part III. Measurement and Reporting. *Chem. Soc. Rev.* **2012**, *41*, 3753−3758.
(48) Møler, J. K. S.; Skibsted, L. H. Nitric Oxide and Myoglobins. *Chem. Rev.* **2002**, *102*, 1167−1178.
(49) Bonnett, R. Photosensitizers of the Porphyrin and Phthalocyanine Series for Photodynamic Therapy. *Chem. Soc. Rev.* **1995**, *24*, 19−33.
(50) Thomas, D. D.; Liu, X.; Kantrow, S. P.; Lancaster, J. R., Jr. The Biological Lifetime of Nitric Oxide: Implications for the Perivascular Dynamics of NO and O_2. *Proc. Natl. Acad. Sci. U. S. A.* **2001**, *98*, 355−360.

DOI: 10.1021/acsami.5b06233
ACS Appl. Mater. Interfaces 2015, 7, 22980−22989